Dalton Transactions

ROYAL SOCIETY OF CHEMISTRY

PAPER

View Article Online
View Journal | View Issue

Cite this: *Dalton Trans.*, 2024, **53**, 6416

The luminescent semiconductor $Pb_7I_6(CN_2)_4$†

Albert T. Schwarz, [a] Markus Ströbele, [a] Carl P. Romao, [b] David Enseling, [c] Thomas Jüstel [c] and H.-Jürgen Meyer *[a]

Received 6th February 2024,
Accepted 12th March 2024

DOI: 10.1039/d4dt00369a

rsc.li/dalton

The development of new compounds in the domain of metal dinitridocarbonates is most efficiently performed *via* solid-state metathesis or simply by addition reactions. Our discovery of $Pb_7I_6(CN_2)_4$ is the result of a solid-state reaction of $PbCN_2$ with PbI_2 at 420 °C. Its crystal structure was solved and refined from X-ray diffraction data based on a single crystal with the space group $P6_3/mmc$. The crystal structure is based on a network of lead tetrahedra, lead trigonal bipyramids and lead octahedra interconnected by $[NCN]^{2-}$ and iodide. Properties of the material were investigated by diffuse reflection measurement, photoluminescence measurements, and electronic band structure calculations demonstrating that this material is a semiconductor.

Introduction

The development of metal dinitridocarbonate compounds is advancing, with many compounds remaining to be discovered. The dinitridocarbonate ion is isolobal to oxygen and thus in some ways analogous to the oxide ion. Generally, the dinitridocarbonate ion can appear as carbodiimide $[N{=}C{=}N]^{2-}$ or cyanamide $[N{\equiv}C{-}N]^{2-}$, depending on the nature and surrounding with cations.

Within the last decades, a remarkable number of metal dinitridocarbonates have been described, most of them having been developed by solid-state metathesis reactions.[1] Many kinds of cations ranging from alkali[2–4] and alkaline earth,[5] transition metal,[6] and a large number of rare earth metals[7,8] have been incorporated; the resulting materials have been studied in terms of their luminescence,[9] magnetism,[10] electrical conductivity,[11,12] and electrochemistry.[13]

Furthermore, complex compounds such as tetracyanamidometallates $[T(NCN)_4]^{n-}$ with T being aluminium,[14] gallium,[15] silicon[16] and germanium[17] have been developed. These materials have shown remarkable photoluminescence properties when combined with a rare earth activator; non-centrosymmetric structures have shown good second harmonic generation (SHG) properties.[16,18] Excellent photoluminescence properties were reported for doped pseudo-binary rare earth (RE) carbodiimides $RE_2(CN_2)_3$,[7,19] such as $RE_2(CN_2)_3$:Ce.[18,20] The structure of the oxide-carbodiimide $Y_2O_2(CN_2)$ is similar to that of the oxide-sulfide Y_2O_2S, which is a well-known host lattice material for photoluminescence.[21] The formal substitution of a chalcogenide *versus* $(CN_2)^{2-}$ is very interesting from a chemical point of view, because it demonstrates that a metal oxide or metal sulfide may serve as a template for the composition of a yet-unknown metal dinitridocarbonate.

The recently discovered compounds $Sn(CN_2)$ and $Sn_2O(CN_2)$ were described as semiconductors with band gaps in the order of 2.0 eV, according to band structure calculations and optical measurements. They have been investigated as a negative electrode material in so-called conversion batteries. Like other transition-metal compounds, carbodiimides $M_x(NCN)_y$ with M = Mn, Cr, Zn have been successfully cycled *versus* lithium and sodium ions.[22]

The diversity of the reported dinitridocarbonate compounds includes several lead-based compounds, such as $Pb(CN_2)$,[23,24] $APb_2Cl_3(CN_2)$ (A = Li, Na, Ag), $LiPb_2Br_3(CN_2)$, $LiPbCl(CN_2)$,[25] $K_{12}Pb_{51}Cl_{54}(CN_2)_{30}$ [26] and $Pb_{14.66}Sn_{7.34}Br_{26}(CN_2)_7O_2$.[27]

In addition, some lead compounds have received special attention over recent years. $CsPbI_3$ can be considered as the archetype for perovskite solar cells following the well-known substitution $(MA)PbI_3$ (MA = CH_3NH_3). $CsPbI_3$ has a bandgap of 1.6–1.8 eV, which is favorable for photovoltaic applications.[28] Other derivatives like $(MA)_2Pb(SCN)_2I_2$, have also been reported.[29] In light of these interesting issues, we herein describe the structure and properties of the new lead carbodiimide iodide $Pb_7I_6(CN_2)_4$.

[a]*Section for Solid State and Theoretical Inorganic Chemistry, Institute of Inorganic Chemistry, University of Tübingen, Auf der Morgenstelle 18, 72076 Tübingen, Germany. E-mail: juergen.meyer@uni-tuebingen.de*
[b]*Department of Materials, ETH Zürich, Wolfgang-Pauli-Str.27, 8093 Zürich, Switzerland*
[c]*Department of Chemical Engineering, FH Münster University of Applied Science, Stegerwaldstraße 39, 48565 Steinfurt, Germany*

†Electronic supplementary information (ESI) available. CCDC 2211751. For ESI and crystallographic data in CIF or other electronic format see DOI: https://doi.org/10.1039/d4dt00369a

Results and discussion

Synthesis

The preparation of crystalline $Pb_7I_6(CN_2)_4$ was performed in a straightforward manner from appropriate (3 : 4) proportions of PbI_2 and $Pb(CN_2)$ heated in fused silica tubes at 420 °C for 5 days (1). This procedure appears to be more efficient than solid-state metathesis, which was used in syntheses of the vast majority of dinitridocarbonate compounds (2). The procedure (1) removes the possibility of incorporation of lithium in the product and avoids the need for leaching significant amounts of the metathesis salt (LiI).

$$3PbI_2 + 4Pb(CN_2) \rightarrow Pb_7I_6(CN_2)_4 \quad (1)$$

$$7PbI_2 + 4Li_2(CN_2) \rightarrow Pb_7I_6(CN_2)_4 + 8LiI \quad (2)$$

$Pb_7I_6(CN_2)_4$ was obtained as a dark yellow crystalline material in high yield, with small amounts of lead being obtained as side phase in the X-ray powder diffraction pattern (Fig. 1).

The side-phase could be a result of the reducing nature of the $(NCN)^{2-}$ ion.[25] EDX measurements on nine different spots on several single crystals revealed a lead to iodine ratio of 7 : 5.96(5), verifying the Pb : I ratio in $Pb_7I_6(CN_2)_4$ that was found in the structure refinement.

Crystal structure of $Pb_7I_6(CN_2)_4$

The crystal structure of $Pb_7I_6(CN_2)_4$ was solved and refined by X-ray diffraction based on recorded single-crystal data. The structure refinement yielded the hexagonal space group $P6_3/mmc$. Some crystal structure and refinement data are given in Table 1.

The crystal structure refinement revealed five crystallographically distinct sites for the lead atoms, with Wyckoff positions, site occupation factors, and atomic coordinates presented in the Table S1.† Pb1 is surrounded by five iodides and three carbodiimide ions, $[NCN]^{2-}$. The environment of Pb2 appears similar to that of Pb1, with one more iodide, forming a coordination pattern derived from a tricapped trigonal antiprism. The third lead site (Pb3) represents a coordination environment with four iodides and three carbodiimide ions. Pb4 is coordinated by three iodine atoms and three $[NCN]^{2-}$ units. Pb5, with a site-occupation factor of 0.75 (see Table S1†), is surrounded by six iodide ions in distorted octahedral formation. Pb–I distances of the distorted octahedron range from 3.0528(6)–3.2555(6) Å. All other Pb–I distances in the drawings outlined in Fig. 2 range from 3.4423(4) Å to 3.7114(8) Å.

The coordination environments of the three crystallographically distinct $[NCN]^{2-}$ units in $Pb_7I_6(CN_2)_4$ are similar to those in the previously reported compound $Pb_{14.66}Sn_{7.34}Br_{26}(CN_2)_7O_2$.[27] Two $[NCN]^{2-}$ units (centred by C1 and C2) are surrounded by six lead ions forming a trigonal antiprismatic arrangement. The third (C3) is surrounded by lead in a trigonal prismatic fashion. A detailed view is shown in Fig. 3.

The Pb–N bond distances range between 2.478(4) and 2.606(4) Å, and are similar to those in the related lead compounds $Pb(CN_2)$ (2.31–2.62 Å),[23] $LiPb_2Cl_3(CN_2)$ (2.54 Å) and $LiPbCl(CN_2)$ (2.39–2.70 Å).[25] The C–N bond lengths of the three crystallographically distinct $[NCN]^{2-}$ units are given in Fig. 3 and appear quite uniform. The C–N lengths around C1 are only slightly different, but the remaining two $[NCN]^{2-}$ are symmetrical, as a result of the a two-fold rotation axis (through C_2) and a mirror plane (cutting C3). Despite minor

Table 1 Selected crystal and structure refinement data for $Pb_7I_6(CN_2)_4$, recorded at 150 K

Empirical formula	$Pb_7I_6(CN_2)_4$
CCDC code	2211751†
Formula weight (g mol^{-1})	5929.62
Wavelength (Mo-K$_\alpha$) (Å)	0.71073
Crystal system	Hexagonal
Space group	$P6_3/mmc$
Unit cell dimensions (Å)	$a = b = 10.7144(1)$
	$c = 29.4426(4)$
Volume (Å^3)	2927.13(7)
Z	5
Density (calculated) (g cm^{-3})	6.728
Absorption coefficient (mm^{-1})	58.057
Final R indices ($I > 2\sigma(I)$)	$R_1 = 0.0212$, w$R_2 = 0.0432$
R indices (all data)	$R_1 = 0.0220$, w$R_2 = 0.0436$
GOOF	1.113

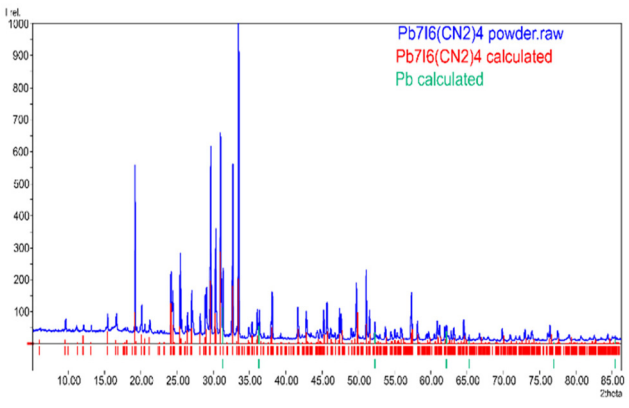

Fig. 1 XRD measurement of compound $Pb_7I_6(CN_2)_4$.

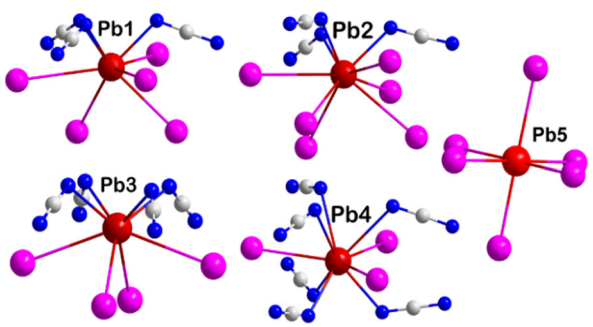

Fig. 2 Different coordination environments of lead atoms in $Pb_7I_6(CN_2)_4$. Iodine is shown in purple, carbon in white and nitrogen in blue.

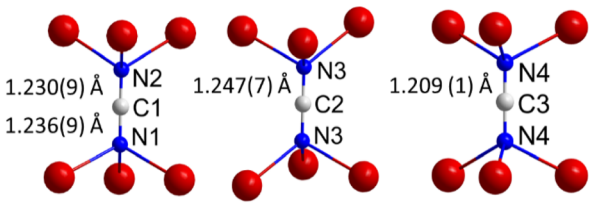

Fig. 3 Three crystallographically distinct $[NCN]^{2-}$ units; two are coordinated nearly trigonal antiprismatic and the third pseudo- octahedrally by lead (red).

differences in length, all three $[NCN]^{2-}$ units can be safely described as carbodiimide ions. An infrared (IR) spectroscopic measurement recorded on a sample of $Pb_7I_6(CN_2)_4$ reveals the presence of three quite similar $[NCN]^{2-}$ units, by showing an asymmetric stretching vibration of the $[NCN]^{2-}$ unit at 1900 cm^{-1} and a C–N bending vibration at 630 cm^{-1} (see Fig. S1†).

An interesting feature in the crystal structure of $Pb_7I_6(CN_2)_4$ is the clustering of lead atoms. A section of the structure showing all five lead atoms is presented in Fig. 4.

The arrangement of lead atoms in the structure may be described as a triple-Pb_4-tetrahedra cluster, composed of three tetrahedra in a face-sharing and edge-sharing fashion, for Pb1–Pb4, or as a trigonal bipyramid with a tetrahedron. All trigonal faces are capped by a nitrogen atom of $[NCN]^{2-}$ (except for the shared one). Pb5 is situated in an octahedral environment of iodide ions. The structure section shown in Fig. 4 is interconnected *via* iodide and carbodiimide ions to form the crystal structure of $Pb_7I_6(CN_2)_4$, as displayed in Fig. 5. Interatomic distances between lead atoms in and between adjacent Pb_4 tetrahedra and with Pb5 range between 3.92(3)–4.23(7) Å. These distances between lead atoms give rise to define block layers within the *ab*-plane in the structure. The given distances are essentially nonbonding distances of Pb^{2+}. However, the distances are significantly shorter than interatomic distances between lead atoms in cubic perovskite structure of $CsPbI_3$, which correspond with the lattice parameter a = 6.2894(2) Å of $CsPbI_3$. This distance resembles the arrangement of edge-shared $[PbI_6]$ octahedra, and is similar with twice the average Pb–I distance (2 × 3.154(1) Å) in the $[PbI_6]$ octahedron of $Pb_7I_6(CN_2)_4$. The surroundings of Pb^{2+} ions in the structure of $Pb_7I_6(CN_2)_4$ do not indicate a lone-pair effect from Pb^{2+}, and the clustering of lead atoms in layers in the structure ultimately suggests some interesting properties.

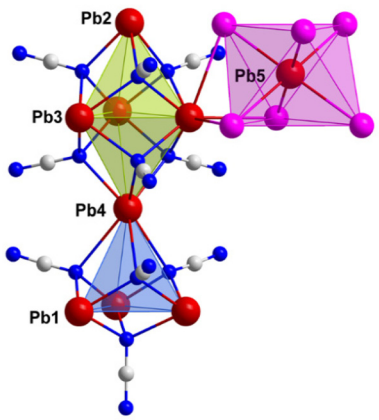

Fig. 4 Face-shared and edge-shared triple-Pb_4-tetrahedra fragment with face-capping carbodiimide ions and an associated $[PbI_6]$ octahedron (purple).

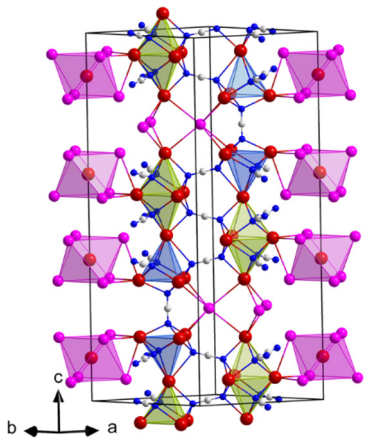

Fig. 5 Section of the crystal structure of $Pb_7I_6(CN_2)_4$. Iodide atoms are shown in purple, lead in red, carbon in white and nitrogen in blue.

Electronic structure

The DFT-calculated electronic band structure of $Pb_7I_6(CN_2)_4$ is shown in Fig. 6. The calculations reveal that the material is an

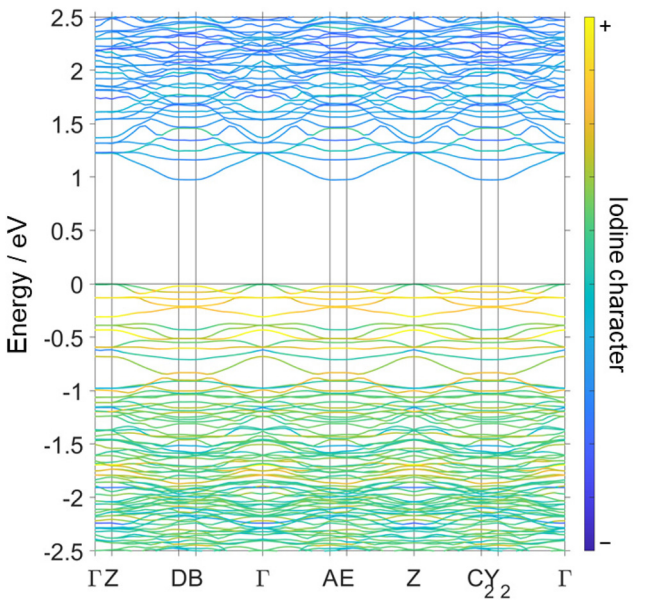

Fig. 6 The electronic band structure of $Pb_7I_6(CN_2)_4$, with bands coloured by their I character. Special points in the Brillouin zone are labelled Γ (0 0 0), Z (0 0 0.5), D (0 0.5 0.5), B (0 0.5 0), A (−0.5 0.5 0), E (−0.5 0.5 0.5), C_2 (−0.5 0.5 0), and Y_2 (−0.5 0 0) and were chosen following literature.[51]

indirect band gap semiconductor, with a gap of about 1 eV. The valence band maximum is close to degenerate (within 0.05 eV) at all special points in reciprocal space; the conduction band minimum is similarly close to degenerate at D (0 0.5 0.5), B (0 0.5 0), A (−0.5 0.5 0), E (−0.5 0.5 0.5), C_2 (−0.5 0.5 0), and Y_2 (−0.5 0 0) points. This result suggests the correct interpretation of the Tauc plot corresponds to an indirect allowed transition with an energy of 2.38 eV (Fig. S2†) rather than a direct allowed transition of 2.47 eV (Fig. S3†). The underestimation of experimental band gaps in DFT is a well-known phenomenon.[30] This problem can be alleviated by the use of hybrid exchange–correlation functionals,[30] however these are significantly more computationally expensive and their use was unfortunately precluded by the large size and low symmetry of the unit cell.

The valence bands near the Fermi energy were found to have significant iodine character (Fig. 6); as in lead halide perovskites.[31] However, the addition of carbodiimide ligands leads to some hybridization of the iodine states with those of nitrogen (Fig. S4†). The complexity of the crystal structure leads to flattening of the electronic bands and, consequently, increased electron localization. It is important to note that, due to this structural complexity and the presence of vacancies, it was not possible to relax the crystal structure in DFT prior to calculating the electronic band structure. This is important as the vacancies would be expected to cause rotation of the coordination polyhedra, which can play an important role in the electronic properties.[32]

Photoluminescence properties

Pb^{2+} comprising compounds are well known for their photoluminescent properties.[33–36] Therefore, an investigation of the photoluminescence properties was carried out, while the excitation and emission spectra of $Pb_7I_6(CN_2)_4$ at 77 K are shown in Fig. 7.

As shown in Fig. 7, the excitation spectrum was observed for monitoring the 525 nm emission and results from the superposition of several sub-bands. More precisely, the spectrum could be resolved into three sub-bands peaking at 302 nm (4.11 eV), 333 nm (3.72 eV), and 378 nm (3.28 eV). As Pb^{2+} is an ns^2 type impurity ion, for the free ion the ground state ($^1S_0$ RS term) arises from the electronic configuration $6s^2$ and the first excited state from the $6s^16p^1$ configuration, consisting of triplet $^3P_{0,1,2}$ and singlet $^1P_1$ states (Fig. 8).[37–39]

Comparison of the measured data with the literature[33,40] suggests that the excitation bands at 302 nm, 333 nm and 382 nm correspond to the transitions from the ground state $^1S_0$ to the excited states $^1P_1$, $^3P_2$ and $^3P_1$ respectively.

The room temperature emission spectra of Pb^{2+}-comprising materials is dominated by a broad emission band, which is typically assigned to the $^3P_1$–$^1S_0$ transition,[37,41] although at low temperatures the strongly forbidden $^3P_0$–$^1S_0$ emission is also observed.[39] The emission spectrum of $Pb_7I_6(CN_2)_4$ at 77 K shows a single broad band peaking at 525 nm (2.36 eV), while the luminescence process is almost completely quenched at 150 K (Fig. 9).

The decay curve of the photoluminescence at 525 nm is almost perfectly monoexponential and yields a decay time of about $\tau_{1/e}$ = 356 ns (Fig. 10).

Since the luminescence of compounds containing the s^2 ion Pb^{2+} is rather diverse, it is useful to compare the found PL data of $Pb_7I_6(CN_2)_4$ with those reported for other Pb^{2+} comprising materials with low and high alkalinity (Table 2).

According to the work of Duffy,[45] the optical alkalinity Λ of Pb^{2+} comprising compounds can be calculated by

$$\Lambda = (60\,700\ \mathrm{cm}^{-1} - \nu)/31\,000\ \mathrm{cm}^{-1}$$

where ν is the energy of the first absorption band in wavenumbers. By definition, this equation yields a Λ value of 1.00 for calcium oxide (CaO). The Λ value of $Pb_7I_6(CN_2)_4$ is found to be 1.10, which points to an optical alkalinity comparable to SrO, which is consistent with the presence of the highly polarizable anions I^- and $(CN_2)^{2-}$in this compound.

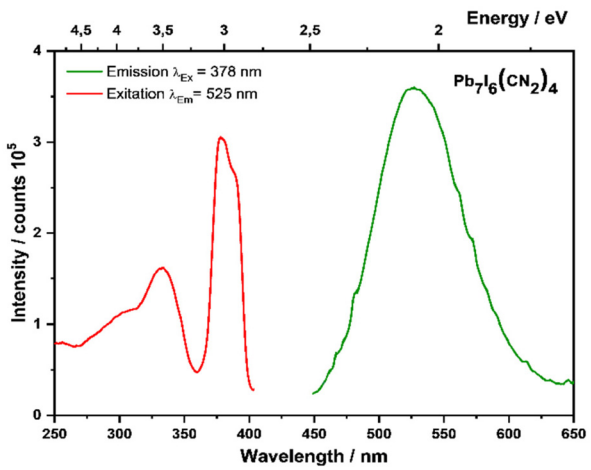

Fig. 7 Excitation and emission spectra of $Pb_7I_6(CN_2)_4$ at 77 K.

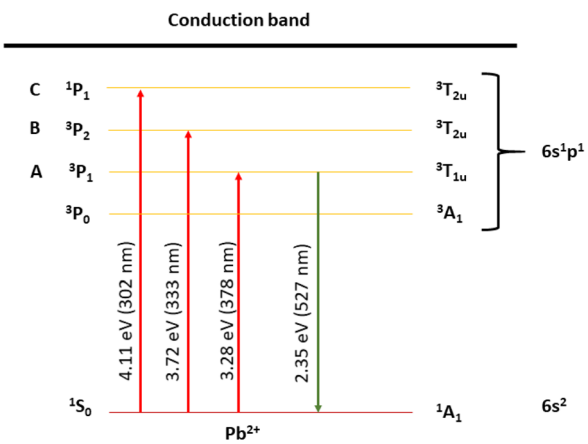

Fig. 8 Energy level scheme of a free Pb^{2+} ion, while the emission occurs from the $^3P_1$ state resulting in a single broad emission band.

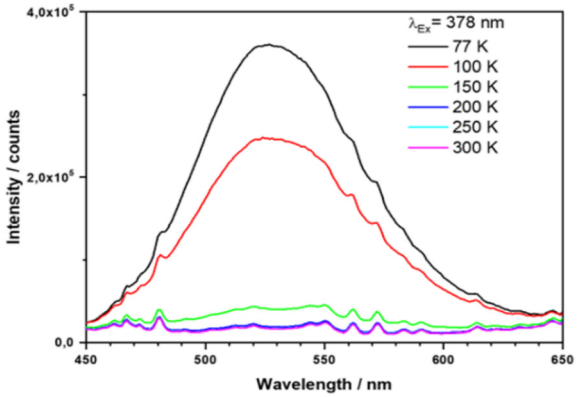

Fig. 9 Temperature dependent emission spectra of $Pb_7I_6(CN_2)_4$ upon 378 nm excitation between 77 and 300 K.

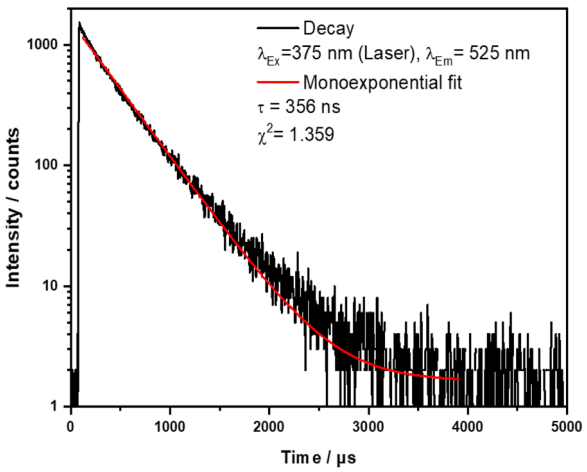

Fig. 10 Decay curve of the 525 nm emission of $Pb_7I_6(CN_2)_4$ at 77 K after excitation at 375 nm.

Table 2 PL data of $Pb_7I_6(CN_2)_4$ and selected lead compounds recorded at low temperature

Composition	Exc. [nm]	Emis. [nm]	Stokes shift [cm^{-1}]	Ref.
$PbSO_4$	235	340	13 000	42
Pb_2OMoO_4	345	525	10 000	43
$Pb_7I_6(CN_2)_4$	378	525	7500	This work
Pb_2OWO_4	340	560	11 500	44

Conclusions

Reactions between lead carbodiimide and lead iodine led to the formation of the previously unknown lead iodine carbodiimide $Pb_7I_6(CN_2)_4$, as confirmed by EDX analysis. Single-crystal X-ray diffraction revealed a complex coordination pattern in the crystal structure, resulting in semiconducting behaviour. Lead atoms form tetrahedral motifs, with an edge-bridging connectivity to a trigonal bipyramid; they can be alternatively viewed as a triple-Pb_4-tetrahedron, with all unoccupied trigonal faces capped by terminally bond carbodiimide ions. Relatively short but nonbonding Pb–Pb distances within these Pb^{2+} clusters give rise to semiconducting behaviour, as determined by band structure calculations. Further electronic properties, such as an evaluation of the photoelectric properties in comparison to the well-known material $(MA)PbI_3$ have not yet been established.

Photoluminescence measurements show the presence of a single broad emission band in the green spectral range with a short decay time of 356 ns at 77 K. The complete quenching at room temperature is likely caused by the large Stokes Shift, which is in line with observations from literature. An emission band of Pb^{2+} at 525 nm points to a highly alkaline environment, which is in good agreement with the high polarizability of the anions of the novel $Pb_7I_6(CN_2)_4$.

Experimental section and calculation details

Synthesis of $Pb_7I_6(CN_2)_4$

Powders of PbI_2 (Sigma-Aldrich, 99.999%) and $PbCN_2$ (synthesized as described in[23]) were mixed and pestled in a glove box under dry argon atmosphere in a 3 : 4 molar ratio. The reaction powder was filled into a silica ampoule and sealed under vacuum. The ampoule was heated in a crucible furnace at 420 °C at a heating and cooling rate of 2 K min^{-1} for 5 d. The reaction product was obtained as a dark yellowish powder with an estimated yield of 90% and lead as a side-phase.

Powder X-ray diffraction

The powder X-ray diffraction pattern was recorded on a well-ground powder in the range $5° < 2\theta < 120°$ using a StadiP diffractometer (Stoe, Darmstadt) with Ge-monochromated Cu-$K_{\alpha1}$ radiation and a Mythen 1 Detector.

Single-crystal X-ray diffraction

Intensity data of single crystals of $Pb_7I_6(CN_2)_4$ were recorded on a Rigaku XtalLAP Synergy-S single-crystal diffractometer, equipped with a HyPix-6000HE detector and monochromatic Mo-Kα radiation. The measurement was performed under N_2 cooling at 150 K. Corrections for absorption effects of the X-ray intensities were applied with a numerical method using CrysAlisPro 1.171.42.64a (Rigaku Oxford Diffraction, 2022). The structure was solved by SHelXL 2018/3 (Sheldrick, 2018) using dual methods and full-matrix least-squares structure refinements implemented in Olex2 1.5-ac5-024.

UV-Vis in diffuse reflectance

The reflectance spectra were recorded on an OceanOptics Maya 2000 Pro spectrometer equipped with a Harrick praying mantis sample chamber. A deuterium tungsten lamp (DH 200 BAL) from OceanOptics was used as the light source. The measurement was performed with the following settings: scan to average = 100, boxcar width = 10 and integration time = 300 ms using OceanView 1.6.7 (lite) software from

OceanOptics. To determine the optical band gap E_g, the Tauc equation was used: $(\alpha \cdot h\nu)^{1/r} = A(h\nu - E_g)$, where α is the absorption coefficient, h is the Planck constant, A is a material related constant and $h\nu$ is the photon energy. For a direct allowed bandgap transition, r = 1/2, and for an indirect allowed bandgap transition, r = 2.

EDX measurements

The energy dispersive X-ray spectroscopy (EDX) were performed with a Hitachi SU8030 scanning electron microscope equipped with a Bruker QUANTAX 6G EDX detector.

Density functional theory (DFT)

Density functional theory (DFT) calculations were performed using the Abinit software package (v. 9)[46] and the Perdew–Burke–Ernzerhof exchange–correlation functional.[47] The electronic structure calculations used the projector-augmented wave (PAW) method[48] with an energy cutoff of 25 Ha outside of the PAW spheres and a 125 Ha cutoff inside them. A 3 × 3 × 2 Monkhorst–Pack grid of k-points was used to sample reciprocal space.[49] Methfessel–Paxton cold smearing of the electronic occupation was included in the calculations.[50] To model the partial occupation of the Pb5 site and respect stoichiometry within the DFT calculations, a Pb5 vacancy was included in the unit cell. The inclusion of this vacancy, along with the structural complexity of the material, precluded structural optimization prior to calculation of the electronic band structure. Special points in and paths through the Brillouin Zone were chosen following Hinuma *et al.*[51]

Photoluminescence

Excitation and emission spectra of $Pb_7I_6(CN_2)_4$ samples were recorded using a fluorescence spectrometer FLS920 (Edinburgh Instruments) equipped with a 450 W xenon discharge lamp (OSRAM) as the radiation source. For powder samples a mirror optic was mounted inside the sample chamber. For the collection of data, a R2658P single-photon-counting photomultiplier tube from Hamamatsu was used. For temperature adjustment a cryostat "MicrostatN" from the company Oxford Instruments had been applied to the present spectrometer. Liquid nitrogen was used as a cooling agent. The photoluminescence decay curve was also measured on the FLS920 spectrometer, while a 375 nm ps laser diode from Edinburgh Instruments was used as an excitation source.

Infrared spectra

Vibrational spectra were recorded with a Bruker Vertex 70 spectrometer within the spectral range from 400to 4000 cm^{-1}; sample were prepared using KBr pellets.

Conflicts of interest

The authors declare no conflict of interest.

Acknowledgements

Support of this research by the Deutsche Forschungsgemeinschaft (DFG-Bonn) through the project ME 914/34-1 is gratefully acknowledged. C. P. R. was supported by ETH Zurich and by the European Union and Horizon 2020 through a Marie Sklodowska-Curie Fellowship, Grant Agreement No. 101030352. Computational resources were provided by ETH Zurich and by the Swiss National Supercomputing Center (CSCS) under project IDs s1128 and eth3.

References

1 H.-J. Meyer, *Dalton Trans.*, 2010, **39**, 5973–5982.
2 M. G. Down, M. J. Haley, P. Hubberstey, R. J. Pulham and A. E. Thunder, *Dalton Trans.*, 1978, 1407–1411.
3 M. Becker, J. Nuss and M. Jansen, *Z. Anorg. Allg. Chem.*, 2000, **626**, 2505.
4 M. G. Down, M. J. Haley, P. Hubberstey, R. J. Pulham and A. E. Thunder, *Dalton Trans.*, 1978, 1407.
5 U. Berger and W. Schnick, *J. Alloys Compd.*, 1994, **206**, 179–184.
6 X. Liu, M. Krott, P. Müller, C. Hu, H. Lueken and R. Dronskowski, *Inorg. Chem.*, 2005, **44**, 3001–3003.
7 M. Neukirch, S. Tragl and H.-J. Meyer, *Inorg. Chem.*, 2006, **45**, 8188–8193.
8 L. Unverfehrt, M. Ströbele, J. Glaser and H.-J. Meyer, *Z. Anorg. Allg. Chem.*, 2009, **635**, 1947–1952.
9 D. Dutczak, A. Siai, M. Ströbele, D. Enseling, T. Jüstel and H.-J. Meyer, *Eur. J. Inorg. Chem.*, 2020, **2020**, 3954–3958.
10 X. Tang, H. Xiang, X. Liu, M. Speldrich and R. Dronskowski, *Angew. Chem., Int. Ed.*, 2010, **49**, 4738–4742.
11 K. Dolabdjian, A. L. Görne, R. Dronskowski, M. Ströbele and H.-J. Meyer, *Dalton Trans.*, 2018, **47**, 13378–13383.
12 M. Löber, K. Dolabdjian, M. Ströbele, C. P. Romao and H.-J. Meyer, *Inorg. Chem.*, 2019, **58**, 7845–7851.
13 Z. Chen, M. Löber, A. Rokicińska, Z. Ma, J. Chen, P. Kuśtrowski, H.-J. Meyer, R. Dronskowski and A. Slabon, *Dalton Trans.*, 2020, **49**, 3450–3456.
14 L. Unverfehrt, M. Kalmutzki, M. Ströbele and H.-J. Meyer, *Dalton Trans.*, 2011, **40**, 9921–9924.
15 M. Kalmutzki, M. Ströbele, S. Kroeker, J. E. C. Wren and H. J. Meyer, *Eur. J. Inorg. Chem.*, 2013, **2013**, 6091–6096.
16 J. Glaser, H. Bettentrup, T. Jüstel and H.-J. Meyer, *Inorg. Chem.*, 2010, **49**, 2954–2959.
17 M. Kalmutzki, D. Enseling, J. E. C. Wren, S. Kroeker, V. V. Terskikh, T. Jüstel and H. J. Meyer, *Inorg. Chem.*, 2013, **52**, 12372–12382.
18 K. Dolabdjian, C. Schedel, D. Enseling, T. Jüstel and H.-J. Meyer, *Z. Anorg. Allg. Chem.*, 2017, **643**, 488–494.
19 J. Glaser, L. Unverfehrt, H. Bettentrup, G. Heymann, H. Huppertz, T. Jüstel and H.-J. Meyer, *Inorg. Chem.*, 2008, **47**, 10455–10460.

20 Y.-C. Wu, T.-M. Chen, C.-H. Chiu and C.-N. Mo, *J. Electrochem. Soc.*, 2010, **157**, J342.
21 J. Sindlinger, J. Glaser, H. Bettentrup, T. Jüstel and H.-J. Meyer, *Z. Anorg. Allg. Chem.*, 2007, **633**, 1686–1690.
22 M. T. Sougrati, A. Darwiche, X. Liu, A. Mahmoud, R. P. Hermann, S. Jouen, L. Monconduit, R. Dronskowski and L. Stievano, *Angew. Chem., Int. Ed.*, 2016, **55**, 5090–5095.
23 X. Liu, A. Decker, D. Schmitz and R. Dronskowski, *Z. Anorg. Allg. Chem.*, 2000, **626**, 103–105.
24 X. Qiao, Z. Ma, D. Luo, A. J. Corkett, A. Slabon, A. Rokicinska, P. Kuśtrowski and R. Dronskowski, *Dalton Trans.*, 2020, **49**, 14061–14067.
25 K. Dolabdjian and H.-J. Meyer, *Z. Anorg. Allg. Chem.*, 2017, **643**, 1898–1903.
26 X. Meng, F. Liang, W. Yin, Z. Lin and M. Xia, *New J. Chem.*, 2019, **43**, 9766–9770.
27 M. Löber, M. Ströbele and H.-J. Meyer, *Z. Anorg. Allg. Chem.*, 2021, **647**, 1973–1977.
28 L. Duan, H. Zhang, M. Liu, M. Grätzel and J. Luo, *ACS Energy Lett.*, 2022, **7**, 2911–2918.
29 M. Daub and H. Hillebrecht, *Angew. Chem., Int. Ed.*, 2015, **54**, 11016–11017.
30 T. Das, G. Di Liberto and G. Pacchioni, *J. Phys. Chem. C*, 2022, **126**, 2184–2198.
31 J. Kaczkowski and I. Płowaś-Korus, *J. Phys. Chem. Lett.*, 2021, **12**, 6613–6621.
32 Y. Huang, W.-J. Yin and Y. He, *J. Phys. Chem. C*, 2018, **122**, 1345–1350.
33 J. Chen, S. Wang, Y. Du and L. Chen, *J. Alloys Compd.*, 2014, **597**, 249–257.
34 W. C. Collins and J. H. Crawford, *Solid State Commun.*, 1971, **9**, 853–856.
35 P. Yang, M. K. Lü, C. F. Song, S. W. Liu, F. Gu and S. F. Wang, *Inorg. Chem. Commun.*, 2004, **7**, 268–270.
36 M. Yılmaz and E. Erdoğmuş, *J. Lumin.*, 2020, **218**, 116868.
37 H. F. Folkerts and G. Blasse, *J. Mater. Chem.*, 1995, **5**, 273–276.
38 H. F. Folkerts and G. Blasse, *J. Phys. Chem. Solids*, 1996, **57**, 303–306.
39 C. P. Joshi and S. V. Moharil, *Phys. Status Solidi B*, 2000, **220**, 985–989.
40 N. Yamashita, T. Ohira, H. Mizuochi and S. Asano, *J. Phys. Soc. Jpn.*, 1984, **53**, 419–426.
41 C. Fouassier, *Curr. Opin. Solid State Mater. Sci.*, 1997, **2**, 231–235.
42 H. F. Folkerts, M. A. Hamstra and G. Blasse, *Chem. Phys. Lett.*, 1995, **246**, 135–138.
43 H. F. Folkerts, J. Zuidema and G. Blasse, *Solid State Commun.*, 1996, **99**, 655–658.
44 R. Alexey, R. Mariana and G. Veronika, *Optik*, 2021, **226**, 165912.
45 J. A. Duffy, *J. Chem. Educ.*, 1996, **73**, 1138.
46 X. Gonze, B. Amadon, G. Antonius, F. Arnardi, L. Baguet, J.-M. Beuken, J. Bieder, F. Bottin, J. Bouchet, E. Bousquet, N. Brouwer, F. Bruneval, G. Brunin, T. Cavignac, J.-B. Charraud, W. Chen, M. Côté, S. Cottenier, J. Denier, G. Geneste, P. Ghosez, M. Giantomassi, Y. Gillet, O. Gingras, D. R. Hamann, G. Hautier, X. He, N. Helbig, N. Holzwarth, Y. Jia, F. Jollet, W. Lafargue-Dit-Hauret, K. Lejaeghere, M. A. L. Marques, A. Martin, C. Martins, H. P. C. Miranda, F. Naccarato, K. Persson, G. Petretto, V. Planes, Y. Pouillon, S. Prokhorenko, F. Ricci, G.-M. Rignanese, A. H. Romero, M. M. Schmitt, M. Torrent, M. J. van Setten, B. Van Troeye, M. J. Verstraete, G. Zérah and J. W. Zwanziger, *Comput. Phys. Commun.*, 2020, **248**, 107042.
47 J. P. Perdew, K. Burke and M. Ernzerhof, *Phys. Rev. Lett.*, 1996, **77**, 3865–3868.
48 M. Torrent, N. A. W. Holzwarth, F. Jollet, D. Harris, N. Lepley and X. Xu, *Comput. Phys. Commun.*, 2010, **181**, 1862–1867.
49 H. J. Monkhorst and J. D. Pack, *Phys. Rev. B: Solid State*, 1976, **13**, 5188–5192.
50 M. Methfessel and A. T. Paxton, *Phys. Rev. B: Condens. Matter Mater. Phys.*, 1989, **40**, 3616–3621.
51 Y. Hinuma, G. Pizzi, Y. Kumagai, F. Oba and I. Tanaka, *Comput. Mater. Sci.*, 2017, **128**, 140.